Electron paramagnetic resonance related to optical charge-transfer processes in ZnSe:Ti

J. Dziesiaty
Humboldt-Universität zu Berlin, Fachbereich Physik, Invalidenstrasse 110, D-10 099 Berlin, Germany

P. Peka, M. U. Lehr, and H.-J. Schulz
Fritz-Haber-Institut der Max-Planck-Gesellschaft, Faradayweg 4-6, D-14 195 Berlin, Germany

A. Klimakow
Institut für Optik und Spektroskopie, Humboldt-Universität zu Berlin, Invalidenstrasse 110, D-10 099 Berlin, Germany
(Received 28 December 1993; revised manuscript received 22 February 1994)

In ZnSe crystals grown by different techniques, titanium ions are incorporated as $Ti^{2+}(d^2)$ and $Ti^{3+}(d^1)$ centers on Zn sites. A strong Jahn-Teller (JT) effect acts on the doubly degenerate ^2E ground state of Ti^{3+}. The electron paramagnetic resonance (EPR) at $T=3$ K indicates a quasistatic JT effect of the ground state and a quasidynamic one of the first excited state for the strain-split vibronic ^2E-$^2A_2$ manifold. These effects are distinguished by their angular variations and the g values. Ti^{2+} causes an isotropic EPR signal. Excitation and sensitization spectra of Ti^{2+} and Ti^{3+} luminescence transitions are explained within a one-electron model connecting internal (d-d) with charge-transfer transitions involving the valence and conduction bands. Both charge states are sensitive to illumination with near-infrared light. The ions can be mutually converted, as shown by photo-EPR and sensitization experiments. The Ti^{2+}/Ti^{3+} donor level is situated approximately 8500 cm^{-1} below the edge of the conduction band.

I. INTRODUCTION

Titanium is a $3d$ transition metal whose ions are known to be incorporated in II-VI and III-V compound semiconductors on cation sites. The impurities form deep-level defects, which are interesting from the technological point of view because of, e.g., photorefractive application in CdTe (high electro-optical coefficient) (Ref. 1) or good thermal stability in III-V compounds (Ref. 2). Since the first successful demonstration of blue-laser action,[3] much interest has been focused on ZnSe as a basic material for a new generation of laser diodes.

Compared with such prominent and extensively studied transition metals as manganese and copper, only a small number of papers have dealt with Ti impurities. Until 1992, in II-VI semiconductors titanium was only observed in the quasineutral oxidation state $Ti^{2+}(d^2)$. The level structure of Ti ions could only be derived from optical absorption measurements; no luminescence was known hitherto. By means of electron paramagnetic resonance (EPR) and luminescence investigations, Klimakow *et al.*[4] detected $Ti^{3+}(d^1)$ ions in addition to $Ti^{2+}(d^2)$ in a II-VI compound (ZnSe). Recently the same experimental methods verified analogous results for Ti in CdTe and (Cd,Zn)Te.[5]

The electronic orbital doublet ^2E, the ground state of a $3d^1$ impurity in a fourfold cubic (T_d) coordination, is expected to undergo a Jahn-Teller (JT) coupling to a twofold degenerate (e type) vibrational mode. The theory of this Jahn-Teller effect in the presence of random strains in the crystals and its implications for the EPR spectra of such d^1 systems have been developed by Ham.[6] He has shown that a description of both the static and the dynamic JT effect can be included in a three-state formulation comprising a vibronic ground doublet and a nearby excited vibronic singlet. EPR studies by Herrington *et al.*[7] on d^1 systems in eightfold cubic coordination can be described by Ham's theory for a weak-to-moderate Jahn-Teller coupling, where the excited singlet is well separated by a large tunneling splitting $3\Gamma \gg \bar{\delta}$ (the strain splitting) from the vibronic ground state ^2E. Boatner *et al.*[8] made use of the three-state theory to account for anomalous features of the $CaO:Ag^{2+}$ spectra by assuming that the strain interaction is of the same order as 3Γ ($3\Gamma \approx \bar{\delta}$), and described the spectra of the equivalent d^9 system in octahedral coordination by an intermediate "quasistatic" Jahn-Teller effect. The only known example of a d^1 impurity in tetrahedrally coordinated II-VI compounds is Sc^{2+} in ZnS, the findings were interpreted in terms of a pure dynamic Jahn-Teller effect ($3\Gamma \gg \bar{\delta}$).[9,10]

In this paper, EPR spectra yield information about the interplay of the static and the dynamic Jahn-Teller effect acting on Ti^{3+}. Using both photo-EPR and sensitization experiments, charge-transfer processes between Ti^{2+} and Ti^{3+} can be detected. By means of excitation spectroscopy, the energy dependence of the efficiency of the different internal or external (charge-transfer) excitation channels is obtained for a defined luminescence transition. In sensitization spectra, the influence of unmodulated light of different wavelengths on the modulated luminescence is measured. Excitation and sensitization spectra thus add knowledge about charge-transfer transitions linking the midgap states with the conduction or

valence bands. These relations are visualized with the help of a one-electron model.

II. EXPERIMENT

The bulk crystals used were produced by two different methods. The first kind of crystal with a diameter of 34×6 mm^2 was grown by a modified Markov method, viz., seeded chemical vapor transport, in hydrogen atmosphere at 1460 K, as described in Ref. 4. Two separate sources of ZnSe and TiSe were used for doping ZnSe with Ti. The crystals of the second charge, with sizes up to $4\times3\times2$ mm^3, were obtained in a sealed ampoule by growth on the powdered (ZnSe+1.5 mol% TiSe) source itself at a constant temperature of 1330 K. In both cases a ZnSe commercial reagent (99.9995% purity) was subjected to vacuum sublimation at 1160 K and preannealed in H_2 at 1270 K to reduce the volatile impurities, to minimize the O_2 content, and to improve the stoichiometry of the starting material. TiSe was synthesized from high-purity elements by increasing the temperature step-to-step from 570 to 1230 K over a two-week period.

Compared with those of the former type, the crystals of the latter charge exhibit higher doping levels of Ti because of smaller growth rates and lower vapor pressure of TiSe. A drawback is their smaller crystal size. For optical and EPR studies, the crystals were prepared by cleaving along the (110) planes.

EPR absorption spectra of the ZnSe:Ti crystals were measured in the temperature range from 3 to 77 K using a homodyne spectrometer working in the X band (9.4 GHz). Optical excitation in the visible spectral range was provided by a high-pressure Hg lamp. The single-crystal samples are oriented by the cleavage face (110) and the well-known very anisotropic spectrum of Fe^{3+} in ZnSe.[11]

The optical measurements were conducted at a temperature of 4.2 K. Xe lamps served as an excitation source; the emitted radiation was detected by means of cooled PbS photoresistors employing a lock-in technique. The radiation from two Xe lamps was directed to the same face of the crystal in an He immersion cryostat. The light emitted from the other side was imaged onto the PbS detector, in front of which optical bandpass filters for a selection of wanted luminescence and for suppression of the exciting beams were mounted. Modulation was effected by a chopper ($f=10-75$ Hz), placed between one of the light sources and the crystal. Directly behind one of the Xe lamps was placed a double-glass-prism monochromator with an automatic constant-power system using a pyrodetector and a slit-width control mechanism. Only this beam was used in recording plain excitation spectra (primary modulated excitation). The second light source with an interference filter for spectral selection was used in excitation experiments with additional excitation (secondary unmodulated excitation). This source could also be used in sensitization experiments, in this case providing the primary modulated excitation. The beam through the monochromator would in this experiment serve as the secondary unmodulated excitation. In all these spectra, the abscissa represents the light provided by the monochromator while on the ordinate the modulated emission flux is plotted, detected in the region defined by the bandpass filters.

III. EPR

A. Theoretical background

For d^2 impurities in tetrahedral coordination (T_d), the free-ion state ^{3}F is split into $^3T_1+{}^3T_2+{}^3A_2$. The $^3A_2$ ground state is an orbital singlet and its behavior in a magnetic field can be described by the simple spin-Hamiltonian

$$\mathcal{H}=g\beta\mathbf{B}\cdot\hat{\mathbf{S}} \tag{1}$$

with isotropic g factor and $S=1$ (Ref. 12).

The free-ion state ^2D of a d^1 impurity is split into a ^2E ground state (orbital doublet) and a $^2T_2$ excited orbital triplet.

The Jahn-Teller effect is here represented by interaction of an electronic E state with e-type vibrational modes.[6] For linear coupling, all the vibronic states are doublets. While the vibronic ground state is of E type, the first excited state is composed of two accidentally degenerate singlets, A_1 and A_2. Through inclusion of nonlinear coupling (warping terms), the levels A_1 and A_2 are repelling each other, so that either A_1 or A_2 approaches the E level, depending on the relative signs of the linear and warping coupling coefficients. In the case of negligible warping, the vibronic singlets are degenerate and the first excited pair, A_1 and A_2, is well removed in energy from the ground doublet, corresponding to the dynamic Jahn-Teller limit where the vibronic ground state is an isolated doublet. The approach of one of the singlets to the ground doublet represents a transition from the dynamic to the static Jahn-Teller limit.

The observed EPR spectra result from the effects of random strain, Zeeman, and hyperfine interactions, on the three lowest vibronic levels. The random strain splitting of the ground doublet is given by

$$\delta=s|V_2|(e_\theta^2+e_\varepsilon^2)^{1/2}, \tag{2}$$

where V_2 is the strain coupling parameter, e_θ and e_ε are the components of the tetragonal strain; $s=(q^2+r^2)^{1/2}$ are reduction factors induced by Ham,[6] which express the change in the expectation values of the anisotropic electronic operators with E symmetry that result from the vibronic coupling. For zero vibronic coupling $q=1$, for strong linear vibronic coupling $q=-r=\frac{1}{2}$, and for strong vibronic coupling with appreciable warping, the relation $q=r/\sqrt{2}<\frac{1}{2}$ is valid.

Usually in bulk crystals the strain splittings are much greater than the anisotropic Zeeman and hyperfine interactions; a magnetic field will act as a perturbation, lifting the remaining degeneracy of each of the three Kramers doublets.

For $3\Gamma\gg\bar{\delta}$ (dynamic JT effect), it leads in first order to two spin transitions corresponding to the anisotropic g factors,[6]

$$h\nu_{\pm}(m)=(g_1\beta B+A_1 m)$$
$$\pm q(g_2\beta B+A_2 m)(1-3\cos^2\theta)\cos^2\varphi\ , \qquad (3)$$

where $\cos\theta$ is the direction cosine of the magnetic field with respect to the cubic crystal axes ($\langle 100\rangle$) and $\tan\varphi=e_\varepsilon/e_\theta$. The coefficients A_1 and A_2 describe the hyperfine coupling to the nuclear spin of quantum number m. The effect of random strains on the EPR spectrum is to distribute the EPR lines between the two extrema given by (3) and leads to a powderlike spectrum exhibiting absorption peaks, which coincide with those expected in the complete absence of strain.

For $\bar{\delta}\gg 3\Gamma$ (static JT effect), the expectation values of the Zeeman interaction are given by three axially symmetric spin Hamiltonians

$$\mathcal{H}_i=\Gamma+g_\parallel\beta B_{z_i}S_{z_i}+g_\perp\beta(B_{x_i}S_{x_i}+B_{y_i}S_{y_i})$$
$$+A_\parallel S_{z_i}I_{z_i}+A_\perp(S_{x_i}I_{x_i}+S_{y_i}I_{y_i})\ , \qquad (4)$$

where $i=1,2,3$ denote the three equivalent [100] axes of the cubic crystal.

The relationships between $g_\parallel$, $g_\perp$, $A_\parallel$, and $A_\perp$ and the effective-Hamiltonian parameters g_1, qg_2, A_1, and qA_2 used to describe the dynamic Jahn-Teller effect are as follows:[6]

$$g_\parallel=g_1\pm 2qg_2,\quad A_\parallel=A_1\pm 2qA_2,\quad g_1=g_0-\frac{4\lambda}{\Delta}\ ,$$
$$g_\perp=g_1\mp qg_2,\quad A_\perp=A_1\mp qA_2,\quad g_2=-\frac{4\lambda}{\Delta}\ . \qquad (5a)$$

(λ is the spin-orbit constant, $\Delta=10Dq$: the parameter of the cubic crystal field.)

For $g_2<0$, the A_2 singlet state is lower. The spin-Hamiltonian (4) corresponds to an EPR spectrum consisting of three magnetically equivalent spectra with tetragonal symmetry, characteristic for the static Jahn-Teller effect,[13]

$$g_\parallel=g_0-\frac{8\lambda}{\Delta},\quad g_\perp=g_0-\frac{2\lambda}{\Delta}\ . \qquad (5b)$$

As the temperature rises and excited states become thermally populated, one may expect additional EPR spectra to appear alongside the spectrum of the ground state. If 3Γ is fairly small, such a spectrum should arise above a few Kelvin, coexisting with the spectrum of the ground state over an appreciable temperature range.

Intermediate effects ($3\Gamma\approx\bar{\delta}$) are manifested by a selective shift and broadening of spectral components relative to an otherwise "pure dynamic" or "pure static" EPR spectrum. The parameters g_1, qg_2, A_1, and A_2 of the effective Hamiltonian can be determined by fitting the angular variations of those spectral components, which are not affected by coupling to the vibronic singlet level (e.g., $g_\perp$ for $qg_2<0$, if the singlet A_2 is the lowest).

For cubic symmetry Setser, Barksdale, and Estle[14] have predicted angular-dependence curves for the ground and excited states for a vibronic ground manifold composed of an E doublet and an A_2 singlet with $qg_2<0$. The Ham reduction parameter ratio q/r takes the strong coupling value of $\sqrt{2}/2$ and the strain parameter φ is assumed to take on all values from 0 to 2π with equal probability. The effect of the singlet on the doublet is contained in the ratio $3\Gamma/\bar{\delta}$. A comparison of these predicted spectra with those measured for certain crystal planes thus allows a determination of $3\Gamma/\bar{\delta}$.

B. EPR results

At $T=3$ K, three spectra of isolated Ti centers are observed.

Spectrum I is characterized by the presence of three tetragonally symmetric complexes, whose principal symmetry axes lie along the three $\langle 100\rangle$ crystallographic axes of the ZnSe crystal. For **B** in a $\{110\}$ cleavage plane, it is possible to observe the resonance spectra for **B** perpendicular to the principal symmetry axes at two different orientations, $\mathbf{B}\|\langle 100\rangle$ and $\mathbf{B}\|\langle 110\rangle$, where the applied field is perpendicular to two of the three sites and to one of the three sites, respectively (Fig. 1).

The g values and hyperfine constants were determined with the magnetic field directed along the $\langle 100\rangle$ crystal axis. In this case, the spectrum is best resolvable and consists of two lines with $g_\parallel=1.8889$ and $g_\perp=1.9620$.

The first line shows hyperfine-structure satellites given by the interaction with ^{47,49}Ti nuclei (5.51% and 7.75% natural abundance and nuclear spin $I=\frac{7}{2}$ and $\frac{5}{2}$, respectively). The corresponding hyperfine coupling constant is $A_\parallel^{\mathrm{Ti}}=(2.60\pm0.05)$ mT. Hyperfine structure of the second line was not so well resolved, so that $A_\perp$ could not be measured. For $\mathbf{B}\|\langle 111\rangle$, the lines coincide at $g_{\langle 111\rangle}=1.937$. From $|A_{\langle 111\rangle}|=(1.7\pm0.1)$ mT, $A_\perp$ was determined as (0.98 ± 0.1) mT.

For the second spectrum, II, the experimentally obtained angular variation in the $\{110\}$ plane ($1\text{-}3\cos^2\theta$) appears to be nearly identical to that expected for systems with dynamic Jahn-Teller effect (Fig. 2). The line shape of each component shows the typical envelope of transitions, which are characteristic of large internal random strains.[6] Because of broadening, no hyperfine structure is resolvable for $\mathbf{B}\|\langle 100\rangle$ and $\mathbf{B}\|\langle 110\rangle$.

Rapid vibronic relaxation between the strain-split components of the vibronic ground state produces an isotropic line by averaging a portion of the strain-broadened

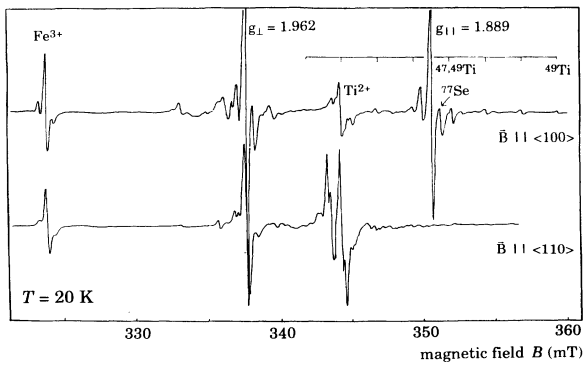

FIG. 1. EPR spectra (I) of Ti^{3+} ($g_\perp=1.962$, $g_\parallel=1.889$) for $\mathbf{B}\|\langle 100\rangle$ and $\mathbf{B}\|\langle 110\rangle$. $T=20$ K. The isotropic Ti^{2+} signal appears at $g=1.9242$.

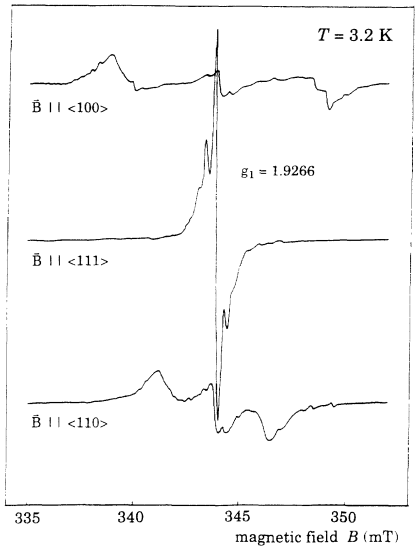

FIG. 2. EPR spectrum (II) of Ti^{3+}, showing "dynamic" Jahn-Teller behavior. $T=3.2$ K. **B** in {110}.

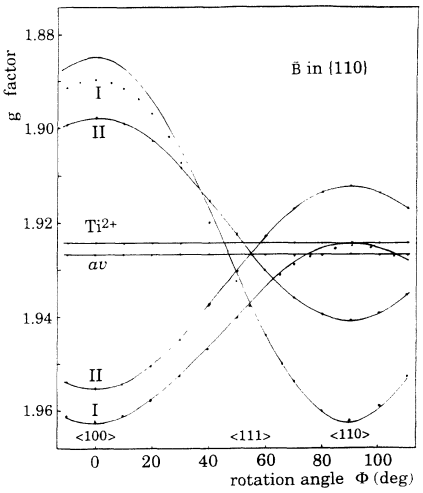

FIG. 3. Angular dependencies of static Jahn-Teller effect (spectrum I), isolated ^2E state (spectrum II), and isotropic Ti^{2+} spectrum in the {110} plane. av, averaged spectrum II; dots, experimental.

resonance pattern.[7] This line at $g_1=1.9266$ has a maximum intensity for $\mathbf{B}\|\langle 111\rangle$ (Fig. 2).

Besides spectra I and II, which are assigned to Ti^{3+}, a third isotropic spectrum is obtained with $g=1.9242\pm0.0005$ (cf. Ref. 15). It is ascribed to Ti^{2+}.

The angular dependences of the lines (Fig. 3) are represented by the solid curves, which are computed using the Hamiltonian for the static Jahn-Teller effect (4) and the effective Hamiltonian for an isolated ^2E state (spectrum II) (3) in the large random-strain approximation. For the appropriate parameters, see Table I.

While the general agreement between theoretical curves and experiment appears to be good, there are some splittings of the complexes at orientations of **B** different from $\mathbf{B}\|[100]$, probably due to slight crystal misalignment.

All three spectra show different saturation behavior. The spectrum with $g=1.9242$ (Ti^{2+}, orbital singlet) is very easily saturated at low temperatures, while spectrum II does not saturate. Therefore, with a certain microwave power not all three spectra are observable simultaneously. With rising temperature, spectrum II is diminished, and above 5 K, only a broad averaged signal at $g=1.9266$ remains up to about 12 K.

Spectrum I is observable up to $T\approx30$ K, but in contrast to spectrum II, no averaged spectrum is observed at $g_{\langle 111\rangle}=1.937$. At temperatures of about 80 K, only the isotropic Ti^{2+} spectrum with $g=1.9242$ remains together with EPR spectra of Fe^{3+} and Mn^{2+}, which are incorporated unintentionally during crystal growth (Fig. 4).

At low microwave power, the main structure consists of a broader line [due to the $\Delta M_S=1$ transitions of the spin Hamiltonian (1), which are inhomogeneously broadened by strains; $\Delta B\approx1.0$ mT] and of a dip (line of inverse phase) situated in the center of the $\Delta M_S=1$ transition at low microwave level. Such a dip was previously found for spin-triplet ground states [Ni^{2+} in MgO (Ref. 16)] and attributed to an internal cross-relaxation mechanism.[17] At higher microwave power, the main structure consists of a sharp $\Delta M_S=2$ double-quantum transition ($\Delta B\approx0.1$ mT) characteristic for a spin triplet ($S=1$).

The partially resolved structure observed on the strong double-quantum transition of the Ti^{2+} spectrum and all transitions of spectrum I and II can be attributed to a

TABLE I. Values of magnetic properties of ZnSe:Ti determined by EPR.

g value	Hyperfine splitting ^{47}Ti, ^{49}Ti (10^{-4} cm^{-1})	Ligand hyperfine splitting ^{77}Se (10^{-4} cm^{-1})
Ti^{3+} (spectrum I), $T=12$ K	$A_\parallel=23\pm0.5$	$A_\parallel=14.5\pm0.5$
$g_\parallel=1.8889\pm0.0005$	($A_\perp=9$)	$A_\perp=8.7\pm0.5$
$g_\perp=1.9620\pm0.0005$	$A_{\langle 111\rangle}=15.5\pm1$	
$g_{\langle 111\rangle}=1.937\pm0.002$		
Ti^{3+} (spectrum II), $T=3$ K		$A_{\langle 111\rangle}=8.5\pm0.5$
$g_2=1.9266\pm0.0006$		
$-qg_2=0.029$		
$q=0.38$		
Ti^{2+}, $T=77$ K	$A=12.5\pm0.5$	$A_\parallel=11.5\pm0.25$
$g=1.9242\pm0.0005$		$A_\perp=9.0\pm0.5$

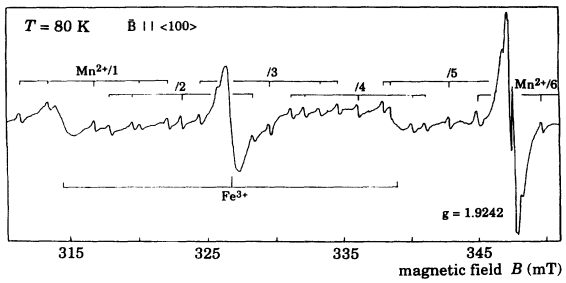

FIG. 4. Ti^{2+} spectrum at 80 K. Impurity spectra of Fe^{3+} and Mn^{2+} are marked. $\mathbf{B}\|\langle 100\rangle$.

hyperfine interaction with the nuclei of four surrounding selenium ions. The only naturally occurring magnetic isotope is ^{77}Se with $I=\frac{1}{2}$ and only 7.5% natural abundance. The probability of finding that more than one of the next Se ions is ^{77}Se is very small. Therefore, the spectrum can be described by the additional term to the spin Hamiltonian

$$\mathcal{H}_{SHF}=\sum_{i=1-4} {}^{77}A_{\parallel}S_{z_i}{}^{77}I_{z_i}+{}^{77}A_{\perp}(S_{x_i}{}^{77}I_{x_i}+S_{y_i}{}^{77}I_{y_i}) , \quad (6)$$

where the z_i direction points from the Ti ions towards the ith Se nucleus. By measuring $|A|$ for $\mathbf{B}\|\langle 100\rangle$, $\langle 110\rangle$, and $\langle 111\rangle$, the values for the spin-Hamiltonian parameters $^{77}A_{\parallel}$ and $^{77}A_{\perp}$ are determined and listed in Table I too.

Under optical excitation, a charge-transfer transition $Ti^{2+}\rightarrow Ti^{3+}$ is observed in the EPR signals (Fig. 5). At low temperatures, optical excitation with $\bar{\nu}\approx 21\,000\ cm^{-1}$ results in an enhancement of the Ti^{2+} signal at $g=1.9242$ by a factor of 2 (depending on the procedure of cooling down) to a ratio of Ti^{2+}/Ti^{3+} of about 1:5, which is stable after the light is switched off. Irradiation with light of energies $\bar{\nu}\leq 15\,000\ cm^{-1}$ decreases the Ti^{2+} signal strongly to $\leq 10\%$ of this value and enhances the Ti^{3+} signal by about 20% (the ratio Ti^{2+}/Ti^{3+} is now approximately 1:60); the signal height is stable again after the light is switched off. Reexcitation with light $\bar{\nu}\geq 21\,000\ cm^{-1}$ restores the Ti^{2+}/Ti^{3+} ratio to its earlier value before the $15\,000\ cm^{-1}$ irradiation. After warming the sample to room temperature in the dark, by cooling back to low temperature the initial ratio of Ti^{2+}/Ti^{3+} of 1:10 is always obtained.

At temperatures above 40 K, only the isotropic signal at $g=1.924$ (Ti^{2+}) is observed, whose intensity is very strongly enhanced (more than ten times) at excitation with $\bar{\nu}\approx 21\,000\ cm^{-1}$ and almost completely quenched with $\bar{\nu}\leq 15\,000\ cm^{-1}$.

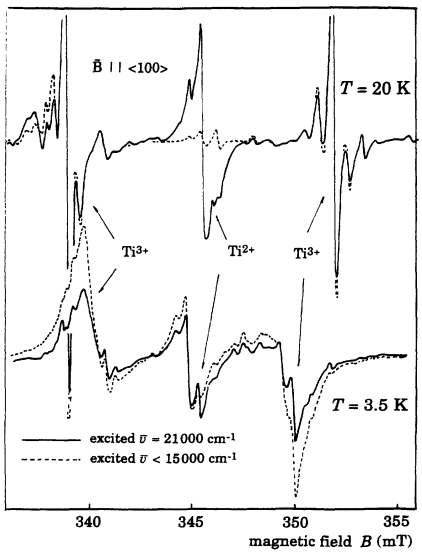

FIG. 5. EPR spectra showing charge transfer by optical excitation. $T=20$ and 3.5 K.

IV. OPTICAL INVESTIGATIONS

The EPR investigations proved that the unilluminated crystals contain $Ti^{2+}(d^2)$ and $Ti^{3+}(d^1)$ simultaneously. Both oxidation states can also be detected by characteristic luminescence transitions. The emission spectrum due to the $^3T_2(F)\rightarrow{}^3A_2(F)$ transition of Ti^{2+} shows a no-phonon doublet[4] at 3436 and 3428 cm^{-1}. The $^2T_2(D)\rightarrow{}^2E(D)$ luminescence of Ti^{3+} peaking near 4300 cm^{-1} has a no-phonon line[4] at 4694 cm^{-1}.

The respective emission bands provide probes to identify the presence and the charge state of titanium ions under specific experimental conditions. Therefore, excitation spectra and changes of optical properties induced by auxiliary irradiation will be studied, also regarding the mentioned light sensitivity of EPR signals (cf. Sec. III). The photonic processes related to photoionization and photoneutralization experiments will be described as schematic reactions, compiled in Table II and graphically represented in Fig. 6. Hence, the underlying idea of a one-electron model of electron transitions will first be introduced.

A. One-electron model

A one-electron model is introduced to demonstrate the complicated system of charge-transfer processes. Al-

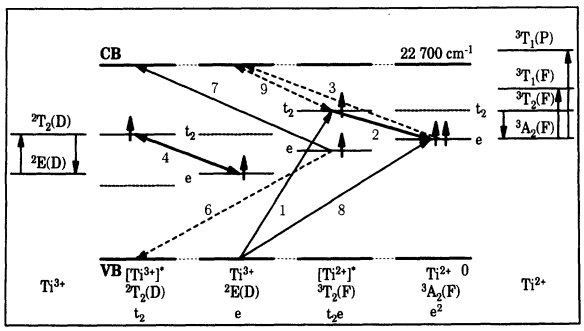

FIG. 6. One-electron model of $Ti^{2+}(d^2)$ and $Ti^{3+}(d^1)$ ions in ZnSe. It contains only ground and first excited states of these ions. For comparison the internal energy levels originating from a many-electron (weak-field) model are sketched on both sides. The numbers represent the reactions discussed in the text and shown in Table II. The dashed transitions are not detected.

TABLE II. Compilation of the charge-transfer processes included in the one-electron model along with the internal transitions (2) and (4) (Fig. 6).

Process No.	Reaction
(1)	$Ti^{3+} + 18\,000\ cm^{-1} \leftrightarrow [Ti^{2+}]^* \equiv {}^3T_2(F) + e^+_{VB}$
(2)	$[Ti^{2+}]^* \leftrightarrow Ti^{2+} + 3400\ cm^{-1}$
(3)	$Ti^{2+} + 8500\ cm^{-1} \leftrightarrow Ti^{3+} + e^-_{CB}$
(4)	$Ti^{3+} + 4700\ cm^{-1} \leftrightarrow [Ti^{3+}]^*$
(5)=(3)+(4)	$Ti^{2+} + 13\,200\ cm^{-1} \rightarrow [Ti^{3+}]^* + e^-_{CB}$
(6)	$[Ti^{2+}]^* \equiv {}^3T_2(F) + e^+_{VB} \leftrightarrow [Ti^{3+}]^* + 12\,900\ cm^{-1}$
(7)	$[Ti^{2+}]^* \equiv {}^3T_2(F) + 9800\ cm^{-1} \leftrightarrow [Ti^{3+}]^* + e^-_{CB}$
(8)	$Ti^{3+} + 15\,000\ cm^{-1} \leftrightarrow Ti^{2+} + e^+_{VB}$
(8)−(4)	$Ti^{2+} + e^+_{VB} \rightarrow [Ti^{3+}]^* + 10\,300\ cm^{-1}$
(9)	$[Ti^{2+}]^* \equiv {}^3T_2(F) + 5100\ cm^{-1} \leftrightarrow Ti^{3+} + e^-_{CB}$

though some drawbacks and simplifications are realized, its advantages are much greater, compared with descriptions placing the weak-field many-electron states of impurity ions into the band gap.

In the center part of Fig. 6, each column consisting of valence-band (VB) maximum, e level, t_2 level, conduction-band (CB) minimum, and electrons on these levels represents a particular state of the Ti ion (corresponding preferentially to one state of the above-mentioned weak-field ladder). Charge-transfer processes are described by arrows connecting the initial and the terminal state of a transition. The number of electrons is only changed on these levels, and just one electron can be actuated with one arrow.

Except for the many-particle schemes added for comparison at the margins, the model contains four separate columns, each representing different oxidation or excitation states. These are from left to right: $[Ti^{3+}]^*$ [corresponding in the weak-field approximation to ${}^2T_2(D)$], Ti^{3+} [which corresponds to ${}^2E(D)$], $[Ti^{2+}]^*$ [here mainly related to the lowest excited state ${}^3T_2(F)$], and Ti^{2+}, viz., ${}^3A_2(F)$. Each substitutional Ti center assumes one of these states, or sometimes one of the higher excited states [e.g., ${}^3T_1(F)$ or ${}^3T_1(P)$ of Ti^{2+}]. These are not included in the model, because it is assumed that they do not play an important role in charge-transfer processes for reasons of fast relaxation to the lower states.

B. Charge-transfer processes

In the excitation spectrum of the $t_2e \rightarrow e^2$ or ${}^3T_2(F) \rightarrow {}^3A_2(F)$ luminescence of Ti^{2+} (Fig. 7), the two dominating peaks at 5950 and 10 050 cm^{-1}, with rising points near 5200 and 9700 cm^{-1}, are due to the known absorption bands from ${}^3A_2(F)$ to ${}^3T_1(F)$ and ${}^3T_1(P)$, respectively.[18–20] The higher state ${}^3T_1(P)$ is degenerate with the conduction band, as concluded earlier from photoconductivity experiments[19] at $T = 300$ K, cf. right-hand many-particle scheme in Fig. 6.

In addition to these "narrow" bands (full width at half maximum of approximately 800 cm^{-1}), the spectrum displays even broader structures in the higher-energy domain. These are related to charge-transfer transitions (which are listed in Table II according to their numbers in Fig. 6) and will be discussed in the following. The increased emission above 17 800 cm^{-1} is assigned to the transition (1) generating $[Ti^{2+}]^*$, which would subsequently relax to the ground state, emitting the characteristic Ti^{2+} luminescence near 3400 cm^{-1} [reaction (2)]. The initial state Ti^{3+} would be finally reached by recombination of Ti^{2+} with the hole created in reaction (1); this is the reverse of process (8) to be discussed below. The peak near 22 000 cm^{-1} in Fig. 7 can be ascribed to an excitation mechanism involving either bound-exciton formation or some unidentified shallow defect level.

With an additional 22 200-cm^{-1} secondary unmodulated irradiation, the spectrum is deformed, viz., the response in the high-energy range is less efficient, because there is a trend toward saturation while excitation in the ${}^3T_1(F)$ and ${}^3T_1(P)$ absorption bands is prevailing.

Under unmodulated 10 000-cm^{-1} secondary irradiation, the excitation spectrum shows exactly the inverse tendency; the Ti^{2+} structures related to the internal absorption bands are diminished, whereas the high-energy range becomes dominant.

The peak near 5300 cm^{-1} in the excitation spectrum of

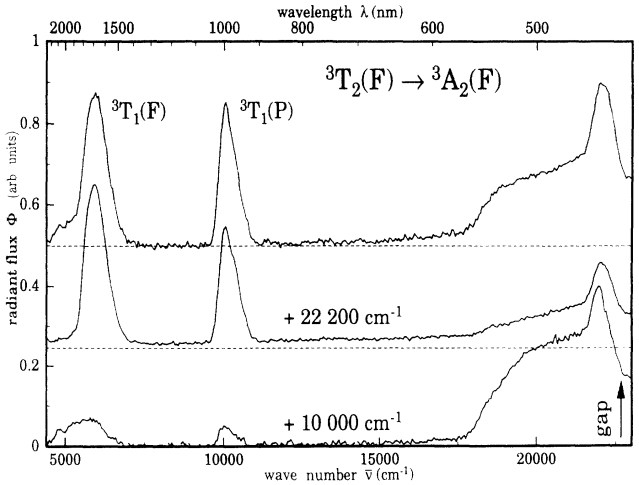

FIG. 7. Excitation spectra of the ${}^3T_2(F) \rightarrow {}^3A_2(F)$ luminescence of $Ti^{2+}(d^2)$ (upper curve). Detected emission range: $\bar{\nu} = 3100$–3300 cm^{-1}. Additional unmodulated radiations: $\bar{\nu} = 21\,400$–$23\,100$ cm^{-1} (middle curve), $\bar{\nu} = 9800$–$10\,200$ cm^{-1} (lower curve). $T = 4.2$ K.

the $t_2 \rightarrow e$ or ${}^2T_2(D) \rightarrow {}^2E(D)$ emission of Ti^{3+} is caused by its resonant excitation (Fig. 8). The rising point near 13 500 cm^{-1} is attributed to a "summation process" proposed here in analogy to a charge-transfer process between Ti^{2+} and Ti^{3+} in GaP (Ref. 21). In ZnSe, the sequence of reactions (3) and (4) is assumed leading to Ti^{3+} excitation [reaction (5)] starting out from Ti^{2+}. After emitting the Ti^{3+} luminescence [inverse of reaction (4)], the system would return to the initial Ti^{2+} ground state, this time by recapture of the conduction electron created in reaction (3) [or (5)]. The energy of 8500 cm^{-1} released in the reversed process (3) is not observed.

The excitation spectrum of the Ti^{3+} emission (Fig. 8) features an ascent near 18 000 cm^{-1} like that of Ti^{2+} (cf. Fig. 7). Again reaction (1) is assumed, this time followed by immediate recapture of the hole [reaction (6)], producing the Ti^{3+} excited state and thus the Ti^{3+} emission detected [reaction (4)]. A weak broad emission band (not shown in this paper) starting around 13 000 cm^{-1} was recorded and can be tentatively assigned to the missing recombination luminescence [reaction (6)]. Finally, a peak occurs in the Ti^{3+} excitation near 22 000 cm^{-1}, as in the case of Ti^{2+}.

Under the influence of an additional irradiation with 20 000 cm^{-1}, a small peak arises near 10 000 cm^{-1} (cf. Fig. 8, upper trace), which coincides with the ${}^3T_1(P)$ absorption band of Ti^{2+} (cf. Fig. 7). The origin of this maximum will be explained later. When the auxiliary irradiation is switched off, this peak is quenched after some minutes, thus restoring the original state of the system as characterized by the lower curve of Fig. 8.

The sensitization spectra under modulation primary low-energy excitation (near 6000 cm^{-1}) exhibit opposite trends for the Ti^{2+} and Ti^{3+} luminescence (Fig. 9). Whereas the Ti^{3+} luminescence is resonantly excited by its inverse absorption, the Ti^{2+} luminescent transition ${}^3T_2(F) \rightarrow {}^3A_2(F)$ is thus excited via the ${}^3T_1(F) \leftarrow {}^3A_2(F)$

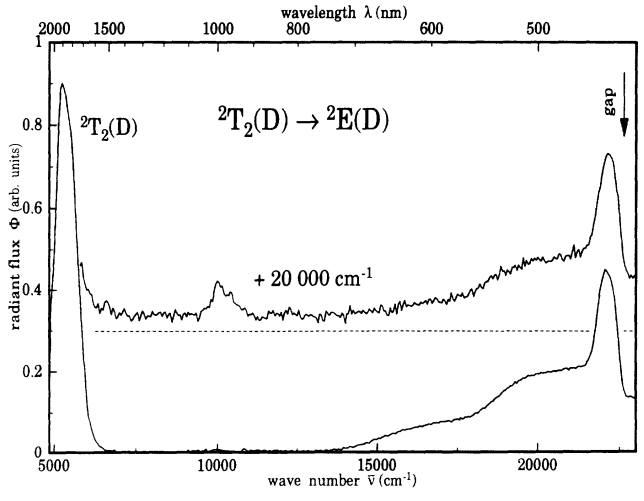

FIG. 8. Excitation spectra of the ${}^2T_2(D) \rightarrow {}^2E(D)$ transition of $Ti^{3+}(d^1)$. Detected emission ranges: $\bar{\nu}=3850-4800$ cm^{-1} (lower curve), $\bar{\nu}=4300-5000$ cm^{-1} (upper curve). Upper curve: additional unmodulated radiation $\bar{\nu}=19\,300-20\,700$ cm^{-1}. $T=4.2$ K.

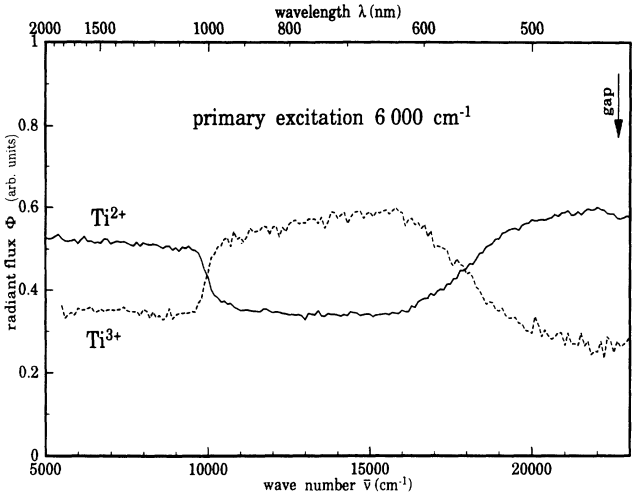

FIG. 9. Sensitization spectra of the ${}^2T_2(D) \rightarrow {}^2E(D)$ luminescence of $Ti^{3+}(d^1)$ (dashed curve) and of the ${}^3T_2(F) \rightarrow {}^3A_2(F)$ transition of $Ti^{2+}(d^2)$ (solid curve). Primary modulated excitation $\bar{\nu}=5850-6200$ cm^{-1}. Detection ranges: $\bar{\nu}=3500-5000$ cm^{-1} (Ti^{3+}), $\bar{\nu}=3100-3600$ cm^{-1} (Ti^{2+}). $T=4.2$ K.

process. Since $T_2 \leftrightarrow A_2$ transitions are symmetry forbidden, the t_2e excited state is expected to be long-living, thus giving rise to absorptions, which lead from ${}^3T_2(F)$ to higher Ti^{2+} levels or to the conduction band. If the energy of the secondary unmodulated irradiation reaches $\bar{\nu} \geq 9500$ cm^{-1}, process (7) and, subsequently, reaction (4) convert Ti^{2+} into Ti^{3+} with the generation of conduction electrons. The radiative Ti^{3+} transition [reaction (4)] is not detected in this sensitization experiment since it is unmodulated. But as a consequence of process (7), under secondary irradiation with $\bar{\nu} \geq 9500$ cm^{-1} the original equilibrium between the concentrations of Ti^{2+} and Ti^{3+} ions is pushed towards Ti^{3+} so that the modulated Ti^{3+} luminescence increases while the Ti^{2+} emission decreases.

On tuning the secondary unmodulated irradiation to $\bar{\nu} \geq 15\,500$ cm^{-1}, the former equilibrium is disturbed towards the opposite direction. Again, both emissions change in a supplementary manner: Ti^{3+} decreases and Ti^{2+} increases, according to process (8).

If the photon energy of the primary modulated excitation is increased to 10 000 cm^{-1}, a completely different sensitization behavior of both emissions is obtained (Fig. 10). In this region, the ${}^3T_2(F) \rightarrow {}^3A_2(F)$ emission of Ti^{2+} is excited via the ${}^3T_1(P)$ level, which is resonant with CB states (cf. Figs. 6 and 7).

The Ti^{3+} center is not directly excited by this photon energy (see Fig. 8); therefore, it starts here (Fig. 10) with zero signal. In principle, process (7) should induce modulated Ti^{3+} emission under modulated 10 000-cm^{-1} excitation. But this excitation mechanism starts out from the $[Ti^{2+}]^* \equiv {}^3T_2(F)$ excited state, which is probably not present in an appreciable concentration under these conditions.

Under secondary unmodulated irradiation with $\bar{\nu} \geq 15\,000$ cm^{-1}, the Ti^{2+} luminescence increases owing

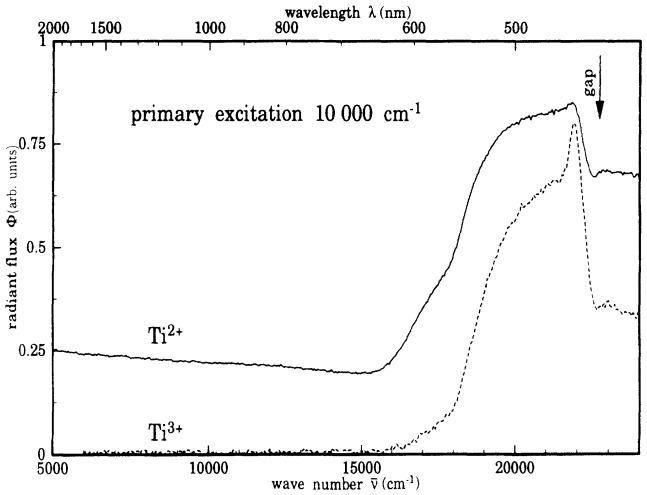

FIG. 10. Sensitization spectra of the $^2T_2(D) \rightarrow {}^2E(D)$ emission of $Ti^{3+}(d^1)$ (dashed curve) and of the $^3T_2(F) \rightarrow {}^3A_2(F)$ transition of $Ti^{2+}(d^2)$ (solid curve). Primary modulated excitation $\bar{\nu}=9800-10\,200$ cm^{-1}. Detection ranges: $\bar{\nu}=3800-4800$ cm^{-1} (Ti^{3+}), $\bar{\nu}=3100-3300$ cm^{-1} (Ti^{2+}). $T=4.2$ K.

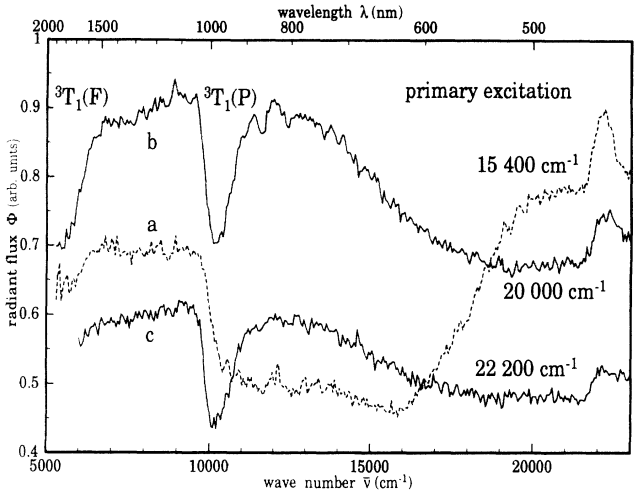

FIG. 11. Sensitization spectra of the $^2T_2(D) \rightarrow {}^2E(D)$ emission of $Ti^{3+}(d^1)$. Primary modulated excitations: (a) 15 050–15 750 cm^{-1}, (b) $\bar{\nu}=19\,300-20\,700$ cm^{-1}, (c) $\bar{\nu}=21\,400-23\,100$ cm^{-1}. Detection range: $\bar{\nu}=3800-4800$ cm^{-1}. $T=4.2$ K.

to process (8). Furthermore, a weak Ti^{3+} emission is now detectable; the increase of Ti^{2+} emission also favors the availability of the $[Ti^{2+}]^*$ state, which is the prerequisite for process (7).

Above 18 000 cm^{-1} the rise in Fig. 10 becomes even steeper. $[Ti^{2+}]^* \equiv {}^3T_2(F)$ is generated directly as a result of reaction (1). This state is partially converted to $[Ti^{3+}]^*$ under the influence of the modulated primary excitation [reaction (7)], leading to a growth of the detection Ti^{3+} emission. In addition, these $[Ti^{2+}]^*$ ions partially decay into an unmodulated Ti^{2+} population, thus permitting modulated excitation by the primary beam, with the result of a further increase of the Ti^{2+} luminescence.

Figure 11 shows another instructive sensitization experiment with the $^2T_2(D) \rightarrow {}^2E(D)$ emission of $Ti^{3+}(d^1)$ under primary modulated excitation of 15 400 cm^{-1} (curve *a*), 20 000 cm^{-1} (curve *b*), or 22 200 cm^{-1} (curve *c*). The interesting point is that the spectra *b* and *c* of Fig. 11 show the $^3T_1(P)$ and $^3T_1(F)$ bands of Ti^{2+}, while spectrum *a* of Fig. 11 has roughly the same shape as the Ti^{2+} sensitization spectrum in Fig. 9.

In the case of curve *a* in Fig. 11, the Ti^{3+} emission is excited directly via the summation process (3)+(4). This reaction requires the ground configuration of Ti^{2+} as the initial state, that is why the spectrum resembles the solid curve in Fig. 9. In both curves, the onsets of the antagonistic processes (7) and (8) are discernible near approximately 9500 and 15 500 cm^{-1}, respectively. The different signs of these directional changes clearly indicate generation of opposite carriers.

In case of *b* of Fig. 11, the Ti^{3+} emission is excited by reaction (1) and subsequent recapture of the hole via process (6). This mechanism requires Ti^{3+} in its ground state as the initial stage; while Ti^{2+} stood at the beginning in case *a* of Fig. 11. In the circle consisting of the processes (1), (6), and (4), one stage [viz., between reactions (1) and (6)] is controversial, that is the long-living first excited state $^3T_2(F)$ or Ti^{2+}. If this state is effectively produced through an unmodulated process (viz., the additional light, represented by the abscissa in Fig. 11), the detected modulated Ti^{3+} signal decreases, since the "unmodulated" $[Ti^{2+}]^*$ states recombine as well with holes via process (6). The various ways of reaching the $^3T_2(F)$ state are given by the excitation spectrum of Ti^{2+} (cf. Fig. 7). Therefore, curve *b* in Fig. 11 looks like an inverted excitation spectrum of Ti^{2+}, the $^3T_1(P)$ and $^3T_1(F)$ bands included.

On the other hand, the circle comprising processes (1), (6), and (4) can be partially broken by the competing reaction (8) commencing from the same initial state as process (1). The number of Ti^{3+} ions in the ground state thus decrease and curve *b* of Fig. 11 declines. The onset of reaction (8) lies at about 15 000 cm^{-1}, but the decline begins near 13 000 cm^{-1} already. The shape of curve *b* near 13 000 cm^{-1} is probably due to a superposition of reaction (8) onto reaction (7) or due to the combined reaction (5), all of which occur in this energy region and depress the modulated signal by producing an unmodulated Ti^{3+} emission.

The spectrum in curve *c* of Fig. 11 has a form similar to curve *b*. This means that either the Ti^{3+} emission is also in this case excited via process (1) and the subsequent reaction (6), or at least the effective excitation channel has the same response to unmodulated additional light as in the case curve *b* of Fig. 11. This channel is probably provided by the generation of bound or free excitons. In fact, in all the spectra of Fig. 11, the near-gap peak at 22 000 cm^{-1} indicates an effective excitation by bound-exciton energy transfer.

V. DISCUSSION

It is assumed that Ti replaces Zn in the ZnSe structure. Titanium can exist in either the Ti^{2+} or Ti^{3+} valence states, depending on whether the Ti donor is neutral or positively charged.

The Ti^{3+} EPR spectra reported here are characteristic of an isolated ^2E state in cubic symmetry. The experimental evidence for strong vibronic interaction is the reduction of certain parameters in the spin Hamiltonians [Eqs. (3) and (4)] with respect to their values predicted by conventional crystal-field theory, which renders the following first-order expressions for a d^1 configuration in tetrahedral coordination:[6]

$$g_1 = 2.0023 - \frac{4\lambda}{\Delta} , \tag{7a}$$

$$g_2 = -\frac{4\lambda}{\Delta} , \tag{7b}$$

$$A_1 = -P\left[\kappa + \frac{4\lambda}{\Delta}\right] , \tag{7c}$$

$$A_2 = -P\left[6\xi + \frac{4\lambda}{\Delta} + \left[\frac{q\lambda}{\Delta}\right]\xi\right] , \tag{7d}$$

with $P = 2\gamma\beta\beta_N\langle r^{-3}\rangle$ and $\xi = \frac{2}{21}$. The parameters λ, Δ, γ, $\langle r^{-3}\rangle$, and κ are the spin-orbit coupling constant, the cubic-crystal-field splitting $10Dq$, the nuclear g factor, the expectation value of r^3, and the Fermi contact parameter, respectively. From Table I, the reduction factor q, included in qg_2 and qA_2, and g_2 may be estimated. For q a value of 0.38 is found, which is smaller than for other d^1 systems in tetrahedrally coordinated compounds. It is distinctly lower than $q = \frac{1}{2}$ and characteristic for strong Jahn-Teller effect with warping.[6]

Taking the $^2T_2 - {}^2E$ distance $\Delta = 4694$ cm^{-1} from luminescence results[4] and the free-ion value $\lambda_0 = 154$ cm^{-1}, a reduction in λ_0 by a factor $k = 0.58$ is obtained, indicating covalence effects ($\lambda/\Delta = 0.019$). Relating these effective Hamiltonian parameters with

$$g_\parallel = g_{\langle 111\rangle} - 2qg_2 = g_0 - \frac{8\lambda}{\Delta} , \tag{8a}$$

$$g_\perp = g_{\langle 111\rangle} + qg_2 = g_0 - \frac{2\lambda}{\Delta} , \tag{8b}$$

to calculate the angular variation for the static Jahn-Teller spectrum (I), there is a difference between g_1 and $g_{\langle 111\rangle}$ due to $2q < 1$, of $\Delta g = (1-2q)2\lambda/\Delta$, $g_{\langle 111\rangle} = g_1 + \Delta g$.

Taking $\Delta g = 0.01$, and $g_{\langle 111\rangle} = 1.937$, the resulting calculated angular variation (Fig. 3) for a slightly lower qg_2 (0.026) is excellent for the branch having a low field extreme, $g_\perp$, at the orientation $\mathbf{B}\parallel\langle 100\rangle$ (spectrum I). The angular variation calculated for the other branch using the same parameters do not fit the experimental points, $g_\parallel$ at $\mathbf{B}\parallel\langle 100\rangle$, indicating an intermediate Jahn-Teller effect near the static limit with $|g_{\parallel(\text{meas})} - g_{\langle 111\rangle}|/qg_2 = 1.8$. The fit corresponds with the predicted values of Setser, Barksdale, and Estle[14] to $3\Gamma/\bar{\delta} \approx 1.5$. Since $qg_2 < 0$, the excited singlet which influences the strain-split E level is A_2. For $3\Gamma/\bar{\delta} = 1.5$, Setser, Barksdale, and Estle[14] predict for the first-excited-state spectrum the shape of a nearly dynamic Jahn-Teller effect. Since the distances between the strain-split doublets are fairly small (about 1 cm^{-1}), they may be populated in the temperature range measured (3–10 K), and indeed both of the spectra have been observed (cf. Fig. 2).

Using a reasonable core polarization constant of $\kappa = 0.66$ for Ti^{3+} and a value of $|P| = (19.3 \pm 1.0) \times 10^{-4}$ cm^{-1} found for Ti^{3+} in MgO (Ref. 22), the hyperfine structure parameter $A_\parallel$ and $A_\perp$ can be calculated to

$$A_\parallel = A_1 + 2qA_2 = 23.8 \times 10^{-4} \text{ cm}^{-1}$$
$$[\text{meas.}\,(23 \pm 0.5) \times 10^{-4} \text{ cm}^{-1}] , \tag{9a}$$

$$A_\perp = A_1 - qA_2 = 9.5 \times 10^{-4} \text{ cm}^{-1}$$
$$[\text{meas.}\,(9 \pm 1) \times 10^{-4} \text{ cm}^{-1}] , \tag{9b}$$

which agree very well with the measurements (cf. Table I).

The measured EPR parameters reported here are all consistent with the following model for Ti^{3+} (Fig. 12).

(i) The ground vibronic state resulting from a strong nonlinear (warping) vibronic interaction ($E_{JT}/\hbar\omega \geq 10$) is a ^2E state with the first excited state A_2 in the order of some cm^{-1} above the ground state ($3\Gamma \approx 1$–2 cm^{-1}).

(ii) Owing to random internal strains the ^2E vibronic state is split into two Kramers doublets, which are separated by about 1 cm^{-1} ($3\Gamma/\bar{\delta} \approx 1.5$).

(iii) The Kramers degeneracy is removed by an applied magnetic field, and the microwave absorption consists of two spectra, arising from the ground state (spectrum I) and the populated first excited state (spectrum II).

(iv) Owing to rapid vibronic relaxation, a portion of the complex envelopes of spectrum II is averaged at temperatures up to 10 K.

Vallin and Watkins[22] discussed the Jahn-Teller effect in $ZnSe:Cr^{2+}$ in terms of interaction with an e mode of $\hbar\omega \approx 50$ cm^{-1}, ascribed to TA(L) (49 cm^{-1}), and a Jahn-Teller energy of about 370 cm^{-1}. With these values taken for $ZnSe:Ti^{3+}$, a rough estimation can be made of 3Γ, $\bar{\delta}$, and Δ'. Ham[6] gives the parameter $\alpha = \hbar\omega$ ($\hbar\omega/4E_{JT}$) as a measure for these energies in the case of strong Jahn-Teller interaction and warping. Use of the values

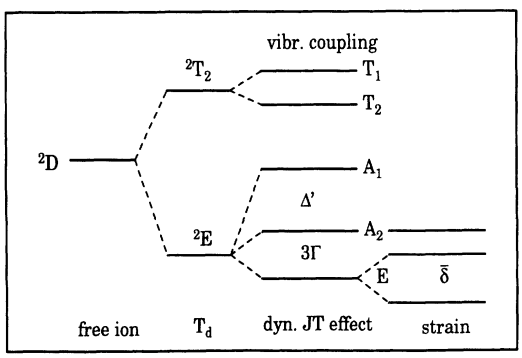

FIG. 12. Energy level diagram of $Ti^{3+}(d^1)$.

above yields $E_{JT}/\hbar\omega \approx 7.5$ and $\alpha \approx 1.6$ cm^{-1}. Since the first excited state should be populated even at temperatures around 3 K, 3Γ should be of the order of 1 cm^{-1} and $3\Gamma/\alpha \approx 0.6$. For the experimental results, $3\Gamma/\bar{\delta} \approx 1.5$ is found and the strain splitting has a value of $\bar{\delta} \approx 0.7$ cm^{-1}. For $3\Gamma/\alpha \approx 0.6$, Ham has calculated $|\beta|/\alpha \approx 5$ and $\Delta'/\alpha \approx 12.5$, where $2|\beta| \approx 16$ cm^{-1} is the barrier height between adjacent wells and $\Delta' \approx 20$ cm^{-1} the distance between A_1 and A_2.

For Ti^{2+} in a tetrahedral environment, a $^3A_2(e^2)$ ground state is expected with properties resembling those of octahedral Ni^{2+} complexes ($t_{2g}^6 e^2$). Thus, the g value should be isotropic and equal $g = g_0 - 8\lambda/\Delta$,[12] where λ is $k\lambda_0$ ($\lambda_0 = 62$ cm^{-1} for Ti^{2+}). Using $\Delta = 3436$ cm^{-1} from luminescence measurements[4] and $k = 0.58$ as estimated for Ti^{3+} above, $g = 1.92$ is obtained, in agreement with the measured g value ($g = 1.9242 \pm 0.0005$). The titanium hyperfine interaction mainly arises from core polarization. Using $\kappa = 0.66$ and

$$|P'| = \{\langle r^{-3}\rangle(Ti^{2+})/\langle r^{-3}\rangle(Ti^{3+})\}|P| = 16.1 \times 10^{-4} \text{ cm}^{-1}, \quad (10)$$

$A = -|P'|(\kappa + \Delta g) = 11.9 \times 10^{-4}$ cm^{-1} results, again in agreement with the measured value of $A = (12.5 \pm 0.5) \times 10^{-4}$ cm^{-1}.

The optical results are discussed in the one-particle model of Fig. 6, which has been introduced especially to illustrate charge-transfer transitions whose energies are derived from experiments. While its basic features are treated in Sec. IV A, some of the more sophisticated implications will be detailed here. One important benefit of the model is the inclusion of four charge-transfer processes connecting $[Ti^{2+}]^* \equiv {}^3T_2$ with the ground or excited state of Ti^{3+} via the conduction band [processes (7) and (9)] or valence band [processes (6) and (1)]. Altogether eight transformations result, counting both directions of the arrows, i.e., emission and absorption processes. The model thus contains some of the previously introduced summation and difference processes. For example, process (1) is the sum of reactions (4) and (6) and also that of reactions (8) and (2).

On the other hand, the model does not include directly (i.e., represented by an arrow) the summation process (3)+(4), or the difference (8)−(4). The initial (two e electrons) and final states (one t_2 electron and one electron in the CB) in the summation process (3)+(4) differ in this model by the positions of two electrons, and therefore, it is impossible to visualize this process with one arrow. The reason lies in the assumptions explained in Sec. IV A.

A fundamental information derived from the model is the position of the Ti^{2+}/Ti^{3+} donor level within the gap. It is defined by process (3), or indirectly by the complementary one, i.e., reaction (8). The sum of the thermal energies of these two processes should yield the gap energy of ZnSe (22 700 cm^{-1}). The tolerance of our estimation of the donor energy is about ± 1000 cm^{-1}, based on the difference between the onsets of the processes in experimental curves and the thermal energies of the transitions. The derived ionization energy referred to the conduction band is 8500 ± 1000 cm^{-1}.

The transition $Ti^{3+} \rightarrow Ti^{2+}$ in the EPR spectra at optical excitation with an energy somewhat below the band gap corresponds to the optical charge-transfer band (rising point 17 800 cm^{-1}) resulting from transition (1) (cf. Fig. 6). The second charge-transfer process, observed in the EPR spectrum under irradiation with light of $\bar{\nu} \leq 15\,000$ cm^{-1} can be ascribed to the optical band rising near 13 900 cm^{-1} [processes (3)+(4)].

The excitation spectra of Ti^{2+} show only a very small band with a rising point around 14 500 cm^{-1} corresponding to process (8). This finding is easy to explain within the model: Process (8) terminates in the ground state of Ti^{2+}; therefore, it cannot generate Ti^{2+} luminescence. But this process pumps negative charge from the VB to Ti^{3+} ions, producing more Ti^{2+} centers, at the expense of those which in the former equilibrium state were in the effectively positive state Ti^{3+}. This $Ti^{3+} \rightarrow Ti^{2+}$ conversion is well demonstrated in the sensitization experiment under 6000-cm^{-1} primary excitation, viz., in the energy range above 15 000 cm^{-1} (cf. Fig. 9).

Sensitization spectra with primary excitation 6000 cm^{-1} show for $\bar{\nu} \geq 9500$ cm^{-1} an increase of Ti^{3+} luminescence and a decrease of the Ti^{2+} emission. The process (7) has been proposed in Sec. IV B, but other channels pumping in the same direction are also possible, e.g., process (9) or process (3), or summation process (3)+(4). All the processes (7), (9), and (3) would push the equilibrium towards the same direction, viz., $Ti^{2+} \rightarrow Ti^{3+}$, but only process (7) turns out to be efficient. A possible explanation is the fact that only process (7) starts and ends in T_2 states, so that strong wave-function interaction is possible. The interaction matrix element is nonzero, since the triple direct product $[T_2 \otimes T_2 \otimes A_1]$ contains A_1, the identity representation of the group T_d. The representation A_1 stands for the free electron released by reaction (7) (cf. Ref. 24). On the other hand, under Laporte's selection rule the efficiency of the process (7) [and also reaction (3)] is decreased because of the d-like behavior of the e level and the s-like character of the conduction band.

The second possible explanation for the excitation of Ti^{3+} via the charge-transfer process with the rising point around 13 500 cm^{-1} (cf. Fig. 8) is the process (8) starting from the VB and Ti^{3+} in its ground state and leading to the e level of the Ti^{2+} ground state while leaving a hole in the VB. The second step of this channel is the so-called "difference process." The hole in the VB recombines with Ti^{2+} to produce $[Ti^{3+}]^*$ in its excited state. The energy released is the difference between the energy involved in process (8) and the energy of the $^2T_2 \rightarrow {}^2E$ internal transition of Ti^{3+}. This process has the same initial and terminal states as the summation process (3)+(4), regarding the ion states. The same conclusions as for the summation process, concerning the impossibility of its simple inclusion into the model, are thus also valid for this difference process. The main distinction between these two complicated processes [(8)−(4) and (3)+(4)] is in the energy band involved. If it is conceded that the summation process exists as a one-photon process, there is no reason why the difference process should not take

place. Based on the experiments made it cannot be decided which one is more efficient. The summation process is supported by its suggested existence[21] in GaP, the difference process by the electric-dipole concession for transitions between p (VB) and d (internal levels) states.

VI. CONCLUSIONS

In the ZnSe crystals investigated, titanium ions are incorporated simultaneously in the charge states $2+$ and $3+$. Contrary to predictions in the literature,[25] a strong dynamic JT effect is found for the ground state ^2E of Ti^{3+} in tetrahedral coordination. The interplay of warping, crystal strains, and magnetic field leads to EPR spectra of the vibronic ground and first excited states of the resulting ^2E-$^2A_2$ manifold, which are observed simultaneously. Near-infrared light illumination can influence the concentration ratio Ti^{2+}/Ti^{3+} which is frozen at low temperatures.

The consistency of EPR and optical results is demonstrated by the good agreement between the measured g values and their estimated values using the crystal-field splitting data from luminescence experiments.

The suggested one-electron model helps to explain even complicated excitation and sensitization experiments by visualizing the charge-transfer processes involved. Especially the demonstrated occurrence of processes (1) and (7) proves the necessity of representing a particular oxidation state of an impurity ion by two different energy levels (t_2,e). The Ti^{2+}/Ti^{3+} donor level is estimated at (8500 ± 1000) cm^{-1} below the edge of the conduction band.

ACKNOWLEDGMENTS

Two of the authors (P.P. and M.U.L.) acknowledge support by stipends of the Max-Planck-Gesellschaft.

[1]R. B. Bylsma, P. M. Bridenbaugh, D. H. Olson, and A. M. Glass, Appl. Phys. Lett. **51**, 889 (1987).

[2]H. Ullrich, A. Knecht, D. Bimberg, H. Kräutle, and W. Schlaak, J. Appl. Phys. **72**, 3514 (1992).

[3]M. Haase, J. Qin, J. De Puydt, and H. Cheng, Appl. Phys. Lett. **59**, 1272 (1991).

[4]A. Klimakow, J. Dziesiaty, J. Korostelin, M. U. Lehr, P. Peka, and H.-J. Schulz, Adv. Mater. Opt. Electron. **3**, 253 (1994).

[5]P. Peka, M. U. Lehr, J. Dziesiaty, S. Müller, J. Kreissl, P. Rudolph, and H.-J. Schulz, Mater. Sci. Forum **143-147**, 435 (1994).

[6]F. S. Ham, in *Electron Paramagnetic Resonance,* edited by S. Geschwind (Plenum, New York, 1972), p. 1.

[7]J. R. Herrington, L. A. Boatner, T. J. Aton, and T. L. Estle, Phys. Rev. B **10**, 833 (1974).

[8]L. A. Boatner, R. W. Reynolds, Y. Chen, and M. M. Abraham, Phys. Rev. B **16**, 86 (1977).

[9]A. O. Barksdale and T. L. Estle, Phys. Lett. **42A**, 426 (1973).

[10]I. Broser and M. Schulz, J. Phys. C **7**, L147 (1974).

[11]J. Dieleman, Philips Res. Rep. **20**, 206 (1965).

[12]A. Abragam and B. Bleaney, *Electron Paramagnetic Resonance of Transition Ions* (Clarendon, Oxford, 1970).

[13]A. Abragam and M. H. L. Pryce, Proc. Phys. Soc. London Sect. A **63**, 409 (1950).

[14]G. G. Setser, A. O. Barksdale, and T. L. Estle, Phys. Rev. B **12**, 4720 (1975).

[15]J. J. Davies, J. E. Nicholls, and D. Verity, J. Phys. C **13**, 1291 (1980).

[16]J. W. Orton, P. Auzins, and J. E. Wertz, Phys. Rev. **119**, 1691 (1960).

[17]S. R. P. Smith, F. Dravnieks, and J. E. Wertz, Phys. Rev. **178**, 451 (1969).

[18]E. M. Wray and J. W. Allen, J. Phys. C **4**, 512 (1971).

[19]K. Kocot and J. M. Baranowski, Phys. Status Solidi B **59**, K11 (1973).

[20]J. M. Baranowski, J. M. Noras, and J. W. Allen, in *Proceedings of the Twelfth International Conference on the Physics of Semiconductors,* edited by M. H. Pilkuhn (Teubner, Stuttgart, 1974), p. 416.

[21]P. Roura, G. Guillot, T. Benyattou, and W. Ulrici, Semicond. Sci. Technol. **6**, 36 (1991).

[22]J. J. Davies and J. E. Wertz, J. Phys. Chem. Solids **31**, 2489 (1970).

[23]J. T. Vallin and G. D. Watkins, Phys. Rev. B **9**, 2051 (1974).

[24]D. J. Robbins and P. J. Dean, Adv. Phys. **27**, 499 (1978).

[25]M. D. Sturge, in *Solid State Physics,* edited by F. Seitz, D. Turnbull, and H. Ehrenreich (Academic, New York, 1967), Vol. 20, p. 91.